Study of a driven self oscillating electrochemical reaction near Hopf bifurcation

F. Berthier[1], J.-P. Diard[2*], B. Le Gorrec[2,3]

[1] Laboratoire d'Étude des Matériaux Hors Équilibres, UMR 8647, Université Paris XI, 91405 Orsay. Fabienne.Berthier@lemhe.u-psud.fr

[2] Laboratoire d'Électrochimie et de Physicochimie des Matériaux et Interfaces, UMR 5631 CNRS-INPG, associé à l'UJF, Domaine Universitaire, BP 75, 38402 Saint Martin d'Hères. erase@lepmi.inpg.fr

[3] Membre de l'Université Joseph Fourier de Grenoble

* Corresponding author

Abstract

The Schuhmann dissolution-passivation (Sdp) model is one of the simplest electrochemical model explaining potential oscillations under galvanostatic conditions. The potential oscillations are due to a Hopf bifurcation. The nonlinear dynamic behaviour of the Sdp model is studied numerically near the Hopf bifurcation. The classical behaviour for forced self oscillating systems such as periodic or quasi periodic behaviours may occur when the current density is modulated by a sinusoidal signal. A phase portrait shows the main Arnol'd tongues where phase locking occurs.

Keywords: Oscillations; Hopf bifurcation; Non-linearity; Arnol'd tongue; Dissolution-passivation model.

1 Introduction

Spontaneous current or electrode potential oscillations often observed when studying the dissolution-passivation of metals such as Fe [1, 2] or electropolishing of metals such as copper [3] have been well documented [4]. Potential oscillations under galvanostatic conditions have also been studied, for example, for the oxidation of formaldehyde [5] and formate [6] on Pt electrodes, the reduction of H_2O_2 on Pt [7] and GaAs [8] and the oxidation of a Ni electrode in H_2SO_4 [9, 10].

The introduction of bifurcation theory has renewed studies on electrochemical oscillators [11]. Forcing an oscillating system with a periodic perturbation is a classical tool to study the behaviour of such systems. Oscillators are then called driven or forced oscillators and their dynamic behaviours are very complex. When the external driving signal is applied, periodic as well as quasi periodic and aperiodic behaviour may occur. Experiments on the bifurcation of periodic states for a forced chemical oscillator have been presented [12]. The bifurcation structure of the driven van der Pol oscillator has been investigated numerically and the phase diagram given for the subharmonic region where the driving frequency is larger than the natural frequency, as well as for the ultraharmonic case where the driving frequency is lower than the natural frequency [13].

Few studies have dealt with the response of oscillating electrochemical systems to periodic forcing apart from the pioneering works of Pagitsas and Sazou. Sinusoidal modulation of the electrode potential in the multisteady-state domain has been studied experimentally for the oxidation of Co [14, 15] and Fe [16, 17]. The current-time responses of these electrochemical oscillators have been studied as a function of the frequency and amplitude of the applied forcing potential. These driven electrochemical oscillators exhibit harmonic and subharmonic as well as quasi periodic current responses. Phase diagrams representing the various types of responses in the amplitude vs. angular frequency perturbating signal plane have been plotted for these two metals. The forced Franck-Fitzhugh model has been studied [18, 18] and shows different types of behaviours depending on the frequency and amplitude of the forcing potential.

The consequences of a saddle-node bifurcation when measuring the impedance of an electrochemical reaction have been studied recently [20, 21, 22, 23]. In order to measure the impedance of an electrode with a frequency response analyser, the electrode potential or the current density is modulated

by adding a small amplitude sinusoidal perturbation. As a result, a self oscillating electrochemical reaction behaves like a driven oscillator when its Faradaic impedance is measured. The consequences of a Hopf bifurcation when modulating the current density is studied in this article based on the example of an oscillating dissolution passivation-model. It is shown that the characteristic behaviours of a driven oscillator, i.e. phase locking and a bi-periodic response, can be observed for the Schuhmann dissolution-passivation (Sdp) model.

2 Schuhmann dissolution-passivation model

The oscillatory behaviour of Ni under galvanostatic conditions has been known for fifty years [9, 10] and the anodic dissolution-passivation of Ni has been widely studied [24, 25, 26, 27, 28]. Most of the mechanisms proposed to explain potential oscillations under galvanostatic conditions take into account a mass transport limitation [29, 30]. A main feature of the anodic dissolution-passivation of Ni is the absence of kinetic limitation by mass transport and it is therefore possible to explain the oxidation of Ni without taking such a limitation into account. D. Schuhmann [31] proposed a kinetic model for anodic metal dissolution in order to explain the shape of the electrode impedance diagrams measured during the oxidation of nickel in acidic media. The Sdp model of a metal involves an intermediate adsorbate X produced by the first step and converted into a passivating species Q in the second step or used as a catalyst in the third and final step. This mechanism is written :

$$\begin{aligned} \mathrm{M,s} &\leftrightarrow \mathrm{X,s} + 2\ \mathrm{e} \\ \mathrm{X,s} &\leftrightarrow \mathrm{Q,s} + 2\ \mathrm{e} \\ \mathrm{X,s} + \mathrm{A} &\rightarrow \mathrm{X,s} + \mathrm{B} + 2\ \mathrm{e} \end{aligned} \tag{1}$$

Assuming, for the sake of simplicity, the irreversibility of the third step, the step rates are given by:

$$v_1(t) = K_{o1}(t)\,\Gamma\,\theta_s(t) - K_{r1}(t)\,\Gamma\,\theta_X(t) \tag{2}$$

$$v_2(t) = K_{o2}(t)\,\Gamma\,\theta_X(t) - K_{r2}(t)\,\Gamma\,\theta_Q(t) \tag{3}$$

$$v_3(t) = K_{o3}(t)\,\Gamma\,\theta_X(t) \tag{4}$$

where:

$$K_{oi}(t) = k_{oi}\,\exp\left(2\,\alpha_{oi}\,f\,E(t)\right)\ ; \qquad K_{ri}(t) = k_{ri}\,\exp\left(-2\,\alpha_{ri}\,f\,E(t)\right)\ ;\ \alpha_{oi} + \alpha_{ri} = 1\ ;\ i = 1, 2 \tag{5}$$

$$K_{o3}(t) = k_{o3}\,\exp\left(2\,\alpha_{o3}\,f\,E(t)\right)\;;\; k_{o3} = k'_{o3}\,A^{*} \tag{6}$$

with $f = F/RT$. The symbols k_{oi}, k_{ri}, α_{oi}, α_{ri}, F, R, and T have their usual meaning. A^{*} is the interfacial concentration of species A assumed to be constant in the electrolyte. The differential equations for θ_X and θ_Q, the fractional surface coverage by the adsorbates X and Q, are given by:

$$\Gamma\,\mathrm{d}\theta_X/\mathrm{d}t = v_1(t) - v_2(t) = K_{o1}(t)\,\Gamma\,\theta_s(t) - K_{r1}(t)\,\Gamma\,\theta_X(t) - \left(K_{o2}(t)\,\Gamma\,\theta_X(t) - K_{r2}(t)\,\Gamma\,\theta_Q(t)\right) \tag{7}$$

$$\Gamma\,\mathrm{d}\theta_Q/\mathrm{d}t = v_2(t) = K_{o2}(t)\,\Gamma\,\theta_X(t) - K_{r2}(t)\,\Gamma\,\theta_Q(t) \tag{8}$$

The Faradaic current density vs. step rate relationship is written:

$$i_f(t) = 2\,F\,\left(v_1(t) + v_2(t) + v_3(t)\right) \tag{9}$$

The steady-state Faradaic current density vs. electrode potential relationship, obtained by writting :

$$\Gamma\,\mathrm{d}\theta_X/\mathrm{d}t = v_1(t) - v_2(t) = 0 \tag{10}$$

$$\Gamma\,\mathrm{d}\theta_Q/\mathrm{d}t = v_2(t) = 0 \tag{11}$$

is given by:

$$i_f = \frac{2\,F\,\Gamma\,K_{o1}\,K_{o3}\,K_{r2}}{K_{o1}\,K_{o2} + K_{r1}\,K_{r2} + K_{o1}\,K_{r2}} = \frac{2\,F\,\Gamma\,K_{o3}}{1 + \dfrac{k_{r1}}{k_{o1}}\exp(-2\,f\,E) + \dfrac{k_{o2}}{k_{r2}}\exp(2\,f\,E)} \tag{12}$$

The bell shape of the current density vs. electrode potential curve is that of a dissolution passivation experimental curve for the chosen set of parameter values as shown in Fig. 1A for one set of parameter values.

The Faradaic impedance $Z_f(E,s) = \Delta E/\Delta i_f$ for the Sdp model (1), calculated using the method proposed by Gerischer and Mehl [32], and developed by Schuhmann [31] and by Epelboin and Keddam [33], is written [34, 35]:

$$Z_f(E,s) = N_{Z_f}/D_{Z_f} \tag{13}$$

with:

$$N_{Z_f} = \left(K_{r1}\,K_{r2} + K_{o1}\,\left(K_{o2} + K_{r2}\right)\right) \times \left(s\,K_{o2} + (s + K_{r1})\,(s + K_{r2}) + K_{o1}\,(s + K_{o2} + K_{r2})\right) \tag{14}$$

and:

$$D_{Z_f} = 4\,f\,F\,\Gamma\,K_{o1}\,K_{r2}\,(K_{o2}\,(K_{o1}\,(s + K_{o3}\,(-1+\alpha_{o3})) + s\,(s + 4\,K_{r1} + K_{o3}\,(-1+\alpha_{o3}))) + (s+K_{r2})\,((s+K_{o3})\,K_{r1} + K_{o3}\,(s + K_{o1} + K_{r1})\,\alpha_{o3})) \quad (15)$$

where s is the Laplace transform operator.

2.1 Linear stability of the Sdp model

The reaction (Eq. (1)) is one of the simplest electrochemical reactions that can explain electrode potential oscillations under galvanostatic conditions. The procedure for studying the linear stability of a two-dimensional non-linear system is to find the eigenvalue of the Jacobean matrix of Eqs. (7) and (8) [36]. This is equivalent to studying the poles of the Faradaic impedance $Z_f(E,s)$, which is the transmittance of the Sdp model under galvanostatic conditions [37, 38, 40, 41]. Poles of the Faradaic impedance are the roots of the Faradaic impedance denominator, i.e. the roots of the equation:

$$D_{Z_f} = 0 \quad (16)$$

Stability under potentiostatic conditions can be studied simply by considering the poles of the Faradaic admittance $Y_f(E,s) = 1/Z_f(E,s)$ or the zeros of the Faradaic impedance. The Faradaic impedance of the reaction (1) is a second-order impedance, i.e. the denominator is a second degree polynomial in the Laplace transform operator s [41]. The two poles of the Faradaic impedance are real or conjugate complex numbers. The steady-state current density vs. electrode potential and the change of the real part of the poles of $Z_f(E,s)$ with the electrode potential are plotted in Fig. 1. The sign of the real part of the poles of the Faradaic impedance shows the stability range of the steady-state under galvanostatic conditions. When the real part of complex poles becomes positive the steady-state becomes unstable under galvanostatic condition. For increasing potential or current density, the poles of the Faradaic impedance are real, complex, then real again (Fig. 1B). The real part of the complex poles becomes positive for $E = E_H$ giving rise to a Hopf bifurcation. The steady-state loses its stability and a stable oscillation encircles an unstable steady-state. The poles becomes real again for a larger electrode potential ($E > E_r$). One of the two real poles becomes negative for the peak electrode potential E_p. The bifurcation diagram showing stable or unstable steady-states and stable periodic oscillations is given in Fig. 1A.

3 Nonlinear dynamic behaviour of the Sdp model

The ordinary differential equation (ODE) for current density is derived from Eq. (9):

$$\mathrm{d}i_f/\mathrm{d}t = 2\,F\,(\mathrm{d}v_1/\mathrm{d}t + \mathrm{d}v_2/\mathrm{d}t + \mathrm{d}v_3/\mathrm{d}t) \tag{17}$$

The nonlinear dynamic behaviour of the electrochemical model (1) can be studied under galvanostatic conditions by solving the 3 dimensional ODE system (Eqs. (7, 8) and (17)) numerically. Neglecting the role of the double-layer capacitance, the change of the Faradaic current density with time for a current density step is given by:

$$\Delta i(t) \approx \Delta i_f(t) = i_f(t) - i_{fi} = \delta i_f \tag{18}$$

where i_{fi} is the initial current density and δi_f the amplitude of the current density step. The change of the Faradaic current density with time for a sinusoidal modulation of the current density is given by:

$$\Delta i(t) \approx \Delta i_f(t) = i_f(t) - i_{fi} = \delta i_f\,\sin(\omega\,t) \tag{19}$$

where δi_f is the sinusoidal modulation amplitude of the current density and ω the driving, perturbating or input angular frequency. The NDSolve function of $Mathematica^{\mathrm{TM}}$ software [42] was used to solve Eqs. (7, 8) and (17) numerically.

4 Self oscillations of the Sdp model

The response of the Sdp model to a small current density step can be obtained using Eq. (13) of the Faradaic impedance and the Laplace transform:

$$\Delta E(s) = Z_f(E,s)\,\Delta i_f(s) = Z_f(E,s)\,\delta i_f/s \tag{20}$$

The linearised model response is calculated by the inverse Laplace transform. This response can be compared to the response calculated numerically from the nonlinear model (Eqs. (7) (8) and (17)).

Linear and nonlinear responses are damped oscillations and are very similar in the stability range of the Sdp model as shown in Fig. 2. Linear and nonlinear responses are very different in the instability range of the Sdp model. Oscillations are undamped for an unstable linear system and bounded for an unstable nonlinear system. Linear and nonlinear responses are compared in

Fig. 3. Nonlinear electrode potential oscillations are sustained bounded in terms of amplitude. Nonlinearities act as return forces and the trajectory of the Sdp model in the θ_X *vs.* θ_X phase plane tends toward a limit cycle. The free oscillating intrinsic or natural Sdp model angular frequency ω_0 can be determined numerically by a Fourier transform. The free frequency oscillation period depends on the electrode potential. It is found that $\omega_0 \approx 32$ rd s^{-1} for an electrode potential $E_M = -0.056$ V. The simulated curves shown in Fig. 2 and 3 and experimental results obtained for nickel in acidic media [9, 10] are very similar in the stability or instabiblity range of the Sdp model.

5 Current density modulation in the instability range of the Sdp model

For a sinusoidal modulation of the input signal of a stable linear system, the output signal is sinusoidal with a period equal to the period T of the input signal. For a sinusoidal modulation of the input signal of a stable nonlinear system, the output signal is periodic with a period equal to the period T of the input signal and includes harmonics with periods equal to $T/2$, $T/3$, etc. Different types of behaviour can be observed for a self-oscillating system. A periodic response with a period equal to the driving signal period T or with a different period may occur. The response may also be quasi-periodic or aperiodic. The response of driven oscillators depends on two angular frequencies, the free frequency and the driven frequency. A signal depending on two independent variables t_1 and t_2 such that $y(t_1, t_2) = y(t_1 + 2\,\pi, t_2)$ and $y(t_1, t_2) = y(t_1, t_2 + 2\,\pi)$ is called bi-periodic. It depends on two fundamental angular frequencies ω_1 and ω_2 or, obviously, two periods. A bi-periodic signal may be periodic or not, depending on whether the ratio of the two fundamental frequencies is rational or irrational [43].

Periodic, quasi-periodic and aperiodic behaviours can be distinguished by their Fourier power spectra [44], or by plotting the Poincaré section. Adding the equation $\mathrm{d}t/\mathrm{d}t = 1$ to Eqs. (10) and (21) transforms a 2 dimensional nonautonomous system into a 3 dimensional autonomous system. The solution of a 3 dimensional autonomous system defines a trajectory in the 3 dimensional space. The attractor of a bi-periodic trajectory is a torus T^2 [12]. The 3D trajectory goes around the torus and can be considered as a combination of two rotations. The orbit sampled every forcing period generates the stroboscopic phase portrait. Strobed points fall on a cross section, the so-called Poincaré section, of the torus. The type of trajectory and its

Poincaré section depend on the ratio ω_1/ω_2. When ω_1/ω_2 is rational, ω_1 and ω_2 are called commensurable, the trajectories are closed curves on the torus and the Poincaré section is made up of a limited number of dots. When ω_1/ω_2 is irrational, ω_1 and ω_2 are called non-commensurable, the trajectories never close, any trajectory can come arbitrarily close to any point on the torus [45] and the Poincaré section is a continuous curve.

The Poincaré section can be plotted using the stroboscopic method to give phase variable values at times that are integer multiples of the driving period [46], i.e. by plotting $\theta_X(k\,T)$ and $\theta_Q(k\,T)$, with integer k, in the θ_X *vs.* θ_Q plane after solving Eqs. (20, 21) numerically. The different behaviours of the driven oscillating Sdp model depending on the ratio ω/ω_0 will be studied in turn.

5.1 Bi-periodic solution

Fig. 4A shows the change of the electrode potential with time for a driving frequency ω of the current density, non-commensurable with respect to the free frequency ($\omega/\omega_0 = \sqrt{2}$). The Poincaré section of the Sdp model trajectory is a continuous curve once initial transients die away due to the fact that the ratio ω/ω_0 is irrational (Fig. 4B). The electrode potential oscillation is not periodic. The Fourier power spectrum shown in Fig. 4C is not made up of peak spectrum. The power spectrum is characteristic of a quasi-periodic signal depending on two frequencies $f_0 = \omega_0/2\,\pi$, the free frequency, and $f = \omega/2\,\pi$, the input signal frequency. In addition to the two principal frequency peaks, the Fourier power spectrum shows peaks for frequencies equal to $|m_0\,f_0 + m\,f|$, m_0 and m being positive or negative integers. The frequency peaks $f - f_0$ and $f + f_0$ are labelled as examples in Fig. 4C. The two frequencies f_0 and f are not commensurable, all the positive numbers are arbitrary close to a combination $|m_0\,f_0 + m\,f|$ and the Fourier power spectra is dense.

5.2 Period-n solution

Fig. 5 shows for the subharmonic case the change of the potential electrode with time for a driving frequency ω of the current density equal to two times the free oscillation frequency ω_0 ($\omega/\omega_0 = 2$; $T = 2\,\pi/\omega = \pi/\omega_0$). After initial transients die away, the second order subharmonic oscillation appears as a sequence of two dots in the Poincaré section (Fig 5B). The potential oscillation power spectrum is made up of discrete peaks and therefore the oscillations are periodic. However the period T_E of the potential oscillations is not equal to the period T of the driving signal, but rather to $2\,T$ as is shown

by comparing current density modulation and potential oscillation (Fig. 5A). Besides the two frequency peaks observed for $f_0 = \omega_0/2\,\pi$ and $f = \omega/2\,\pi$, the potential Fourier power spectrum shows peaks for frequencies equal to $|m_0\,f_0 + m\,f|$. The frequency ratio is rational with $f/f_0 = 2$. Fourier power spectrum is made up of discrete peaks corresponding to harmonics of the frequency $f - f_0 = f/2$. This well known phenomenon for driven oscillators is called phase-locking. Multiplication of the period by two is due to frequency ratio value and should not be confused with the so-called period-doubling bifurcation route to chaos. Obviously multiplication of the period by three will be observed for $\omega/\omega_0 = 3$. For $\omega/\omega_0 = 2$, the angular frequency ω_E of the electrode potential oscillation is equal to ω_0 since $T_E = 2\,T$ is equivalent to $\omega_E = \omega_0$.

The Sdp model imposes its free oscillation frequency for a sufficiently small modulation amplitude δi_f and obviously the potential oscillation frequency is equal to the free frequency for $\delta i_f = 0$. For increasing modulation amplitudes, multiplication of the input signal period by two is observed not only for driven periods equal to exactly two times the free oscillation period but also for values near two. Multiplication of the input signal period by two is observed in Fig. 6 for ω/ω_0 ($T = 2\,\pi/\omega = \pi/1.1\,\omega_0$). The period of the potential oscillation is still equal to two times the driven period but not to the free oscillation period since is equivalent to $\omega_E = 1.1\,\omega$. Mode locking occurs for a certain set of δi_f and ω/ω_0 values. Regions in the δi_f *vs.* ω/ω_0 plane where mode locking occurs are called Arnol'd tongues [13].

Multiplication of the input signal period by an integer number is also obtained for any driving frequency integer multiple of the free frequency ω_0, and in a more general way for any frequency commensurable with respect to ω_0, *i.e.* where $\omega/\omega_0 = n/m$, where n and m are small integers. The period of the mode-locked solution is n times the period of the driving signal. This behaviour is shown in Fig. 7 for $\omega/\omega_0 = 2/3$ ($T = 2\,\pi/\omega = 3\,\pi/\omega_0$) for the ultraharmonic case where the driving frequency is lower than the Sdp model free frequency. The response is periodic and the period is neither the period of the driving current density nor the free oscillation period but is equal to two times the driving period. For $\omega/\omega_0 = 2/3$, the angular frequency of the electrode potential oscillation is equal to a third of the free angular frequency since $T_E = 2\,T$ is equivalent to $\omega_E = \omega/2 = \omega_0/3$.

An Arnol'd tongue for period-2 solution then originates from the point with abscissa $\omega/\omega_0 = \omega/2 = 2/3$. In a more general way, an Arnol'd tongue originates for $\delta i_f = 0$ from every point where the driving frequency is a

rational multiple of the free frequency, *i.e.*, whenever $\omega/\omega_0 = n/m$, where n and m are integer numbers. Other tongues exists between these tongues since for rational n_1/m_1 and n_3/m_3, $n_2/m_2 = (n_1 + n_3)/(m_1 + m_3)$ is also rational with $n_1/m_1 < n_2/m_2 < n_2/m_3$. For the chosen example, an Arnol'd tongue can be predicted for $\omega/\omega_0 = 1$, from those obtained for $\omega/\omega_0 = 2/3$ and $\omega/\omega_0 = 2$ since $(2 + 2)/(3 + 1) = 1$. The angular frequency of the electrode potential oscillation is equal to the free angular frequency.

Arnol'd tongues do not grow indefinitely with increasing δi_f and for a sufficiently high δi_f there exists only a single stable period-one solution and the potential oscillation period is equal to the input current density period.

5.3 Period-1 solution

Fig. 8 shows the change of the potential electrode with time for a driving frequency ω of the current density equal to two times the free oscillation frequency ω_0. Period multiplication disappears with increasing amplitude modulation δi_f, when the driving frequency is kept constant, as shown in Fig. 8A for $\delta i_f = 3\ 10^{-3}$ A cm^{-2}. Potential oscillation is periodic and the period is equal to the driving period (Fig. 8A). The Poincaré section is made up of one dot after initial transients die away (Fig. 8B). The Fourier power spectrum is made of discrete peaks corresponding to harmonics of the driving frequency (Fig. 8C). The power of the driving modulation is such that the Sdp model follows the driving signal. This behaviour closes the Arnol'd tongues for a sufficiently high amplitude modulation as shown in Fig. 9. Three principal Arnol'd tongues, obtained for small values of n and n_0, are shown in Fig. 9.

6 Conclusion

It has been shown that the Sdp model behaves like a classical forced self-oscillating system when the faradaic current density is modulated in its instability range. When the Faradaic current density is modulated in the stability range of the Sdp model the electrode potential is modulated with a period equal to the current density modulation. When the Faradaic current density is modulated in the instability range, the electrode potential oscillations may be periodic with a period equal to the period of the modulation faradaic current density or n times the modulation period or quasi-periodic, *i.e.* bi-periodic.

When the potential oscillation is periodic with a period of n times the

driving period, mode locking behaviour occurs. The areas in the plane δi_f *vs.* ω/ω_0 where mode locking occurs are Arnol'd tongues. An Arnol'd tongue originates from every point where the driving frequency is a rational multiple of the free frequency, *i.e.* for all $\omega/\omega_0 = n/m$. Arnol'd tongues are closed by period-1 electrode potential oscillations for sufficiently high amplitude values. Therefore to obtain electrode potential oscillations with a period equal to the period of the current density it is necessary to choose a sufficiently high value of the amplitude modulation in contradiction with the necessity of using a sufficiently low amplitude for impedance measurements.

Electrochemical reaction impedance is usually measured in a logarithmic mode over a wide frequency range with a low amplitude modulation of potential or current density. Therefore bi-periodic behaviour can be predicted. The consequences of bi-periodic behaviour on impedance measurements are far from obvious. A driven oscillator such as a van der Pol oscillator exhibits deterministic chaos [13]. For the time being, this behaviour has not been found for the Sdp model. Bifurcation between different forced Sdp model behaviours is beyond the scope of this article and will be studied further using the first return map in the Poincaré section.

References

[1] Russell, P.; Newman, J. J. Electrochem. Soc., 134 1987 1051.

[2] Lou, W.; Ogura, K. Electrochim. Acta, 40 1995) 667.

[3] Pointu, P.; Braizaz, M.; Poncet, P.; Rousseau, J. J. Electroanal. Chem. 122 1981 111.

[4] Wojtowicz, J. Modern Aspect of Electrochemistry; Bockris, J.O'M.; Conway, B.E., Eds.; Butterworths, London, 1972.

[5] Xu, Y.; Schell, M. J. Phys. Chem., 94 1990 7137

[6] Albahadily, F. N.; Schell, M. J. Electroanal. Chem., 308 1991 151.

[7] van Venrooij, T. G. J.; Koper, M. T. M. Electrochim. Acta, 40 1995 1689.

[8] Koper M. T. M.; Vanmaekelbergh, D. J. Phys. Chem., 99 1995 3687.

[9] Hoar, T. P.; Mowat, J. A. S. Nature (London), 165 1950 64.

[10] Osterwald J.; Feller, H. G. J. Electrochem. Soc., 107 1960 473.

[11] Koper, M. T. M. Advances in Chemical Physics, vol XCII 1996 161.

[12] Vance, W.; Ross, J. J. Chem. Phys. 88 1988 5536.

[13] Mettin, R.; Parlitz, U.; Lauterborn, W. Int. J. Bifurcation and Chaos, 3 1993 1529.

[14] Pagitsas, M.; Sazou, D. J. Electroanal. Chem., 386 1995 88.

[15] Pagitsas, M.; Sazou, D. Electrochim. Acta, 40 1995 755.

[16] Sazou, D.; Karantonis, A.; Pagitsas, M. Int. J. of Bifurcations and Chaos, 3 1993 981.

[17] Karantonis, A.; Pagitsas, M.; Sazou, D. Chaos, 3 1993 243.

[18] Pagitsas, M.; Sazou, D. Electrochim. Acta, 36, 1991 1301.

[19] Pagitsas, M.; Karantonis A.; Sazou, D. Electrochim. Acta, 37 1992 1047.

[20] Berthier, F.; Diard J.-P.; Montella, C. J. Electroanal. Chem, 410 1996 247.

[21] Berthier, F.; Diard J.-P.; Montella, C. J. Chim. Phys., 95 1998 1101.

[22] Berthier, F.; Diard J.-P.; Le Gorrec, B.; Montella, C. J. Electroanal. Chem., 458 1998 231.

[23] Berthier, F.; Diard J.-P.; Montella, C. J. Electroanal. Chem., 460 1999 226.

[24] Epelboin, I.; Keddam, M. Electrochim. Acta, 17 1972 177.

[25] Jouanneau, A.; Keddam M.; Petit, M. C. Electrochim. Acta, 21 1976 287.

[26] Keddam, M.; Takenouti H.; Yu, N. J. Electrochem. Soc., 132 1985 2561.

[27] Lev, O.; Wolffberg, A.; Pismen L. M.; M. Sheintuch, L. M. J. Phys. Chem., 93 1989 1661.

[28] Haim, D.; Lev, O.; Pismen L. M.; Sheintuch, M. J. Phys. Chem. 96 1992 2676.

[29] Koper M. T. M.; Sluyters, J. H. J. Electroanal. Chem., 371 1994 149.

[30] Strasser, P.; Lübke, M.; Eickes C.; Eiswirth, M. J. Electroanal. Chem., 462 1996 19.

[31] Schuhmann, D. J. Electroanal. Chem., 17 1968 45.

[32] Gerischer H.; Mehl, W. Z. Elecktrochem., 59 1955 1049.

[33] Epelboin I.; Keddam, M. J. Electrochem. Soc., 117 1970 1052.

[34] Berthier, F.; Diard J.-P.; Landaud P.; Montella, C. J. Electroanal. Chem., 362 1993 13.

[35] Diard J.-P.; Le Gorrec, B.; Montella, C. Cinétique Électrochimique, Hermann, Paris, 1996.

[36] Glendinning, P. Stability, Instability and Chaos, Cambridge University Press, Cambridge, 1994.

[37] Koper, M. T. M. J. Electroanal. Chem. 409 1996 175.

[38] Alonzo, V.; Berthier, F.; Diard J.-P.; Seignole, V. J. Chim. Phys., 94 1997 1763.

[39] Berthier, F.; Diard J.-P.; Montella, C. C. R. Acad. Sci. Paris 325 1977 21.

[40] Berthier, F.; Diard J.-P.; Montella, C. Electrochim. Acta, 44 1999 2397.

[41] Diard J.-P.; Le Gorrec, B.; Montella, C.; Montero-Ocampo, C. J. Electroanal. Chem., 352 1993 1.

[42] Wolfram, S. Mathematica^{TM}, Addison-Wesley, Redwood City, 1988.

[43] Seydel, R. Practical bifurcation and stability analysis, Springer-Verlag, New Yorg, 1994.

[44] Bergé, P.; Pomeau, Y.; Vidal, C. L'ordre dans le chaos, Hermann, Paris, 1984.

[45] Hale J.; Koçak, H. Dynamics and Bifurcations, Springer-Verlag, New-York, 1991

[46] Thomson J. M. T.; Stewart, H. B. Nonlinear Dynamics and Chaos, John Wiley and Sons, Chichester, 1987.

Figure captions

Fig. 1. Steady-state current density vs. electrode potential for $k_{o1} = 500$ s^{-1}; $k_{r1} = 10$ s^{-1}; $\alpha_{o1} = 0.95$; $\alpha_{r1} = 1 - \alpha_{o1}$; $k_{o2} = 100$ s^{-1}; $k_{r2} = 1$ s^{-1}; $\alpha_{o2} = 0.2$; $\alpha_{r2} = 1 - \alpha_{o2}$; $k_{o3} = 10^3$ s^{-1}; $\alpha_{o3} = 0.2$; $\Gamma = 10^{-9}$ mol cm^{-2}. A: Solid line: stable steady-states under galvanostatic conditions, dashed line: unstable steady-states, dot: minimum and maximum of electrode potential oscillations. B: Change of the poles real part of the Faradaic impedance with the electrode potential. Stable steady-states, dots: stable potential oscillations. E_M = –0.056 V.

Fig. 2. Linear (A) and nonlinear (B) responses to a current density step in the stable range. C: Phase plane portrait.

Fig. 3. Linear (A) and nonlinear (B) responses to a current density step in the unstable range. C: Phase plane portrait.

Fig. 4. Electrode potential response to a current density modulation. A: current density modulation (high) and electrode potential oscillation (low), B: Poincaré section in the $\Delta\theta_Q = \theta_Q(t) - \theta_{Qi}$ *vs.* $\Delta\theta_X = \theta_X(t) - \theta_{Xi}$ plane, C: potential oscillation Fourier power spectrum. $\omega/\omega_0 = \sqrt{2}$; $\delta i_f = 0.4$ mA cm^{-2} ; k = 400.

Fig. 5: Electrode potential response to a current density modulation. A: Current density modulation (high) and electrode potential oscillation (low), B: Poincaré section in the $\Delta\theta_Q = \theta_Q(t) - \theta_{Qi}$ *vs.* $\Delta\theta_X = \theta_X(t) - \theta_{Xi}$ plane, C: potential oscillation Fourier power spectrum. $\omega/\omega_0 = 2$; $\delta i_f = 0.2$ mA cm^{-2} ; k = 400.

Fig. 6. Electrode potential response to a current density modulation. A: Current density modulation (high) and electrode potential oscillation (low), B: Poincaré section in the $\Delta\theta_Q = \theta_Q(t) - \theta_{Qi}$ *vs.* $\Delta\theta_X = \theta_X(t) - \theta_{Xi}$ plane, C: potential oscillation Fourier power spectrum. $\omega/\omega_0 = 2.2$; $\delta i_f = 0.6$ mA cm^{-2}.

Fig. 7. Electrode potential response to a current density modulation. A: Current density modulation (high) and electrode potential oscillation (low), B: Poincaré section in the $\Delta\theta_Q = \theta_Q(t) - \theta_{Qi}$ *vs.* $\Delta\theta_X = \theta_X(t) - \theta_{Xi}$, C: potential oscillation Fourier power spectrum. $\omega/\omega_0 = 2/3$; $\delta i_f = 0.8$ mA cm^{-2}.

Fig. 8. Electrode potential response to a current density modulation. A: Current density modulation (high) and electrode potential oscillation (low), B: Poincaré section in the $\Delta\theta_Q = \theta_Q(t) - \theta_{Qi}$ *vs.* $\Delta\theta_X = \theta_X(t) - \theta_{Xi}$ plane, C: potential oscillation Fourier power spectrum. $\omega/\omega_0 = 2$; $\delta i_f = 3$ mA cm^{-2}.

Fig. 9. Arnol'd tongues for the Sdp model. n ($n = 1$, 2) indicates a period-n stable regime. Encircled numbers indicate corresponding figure.

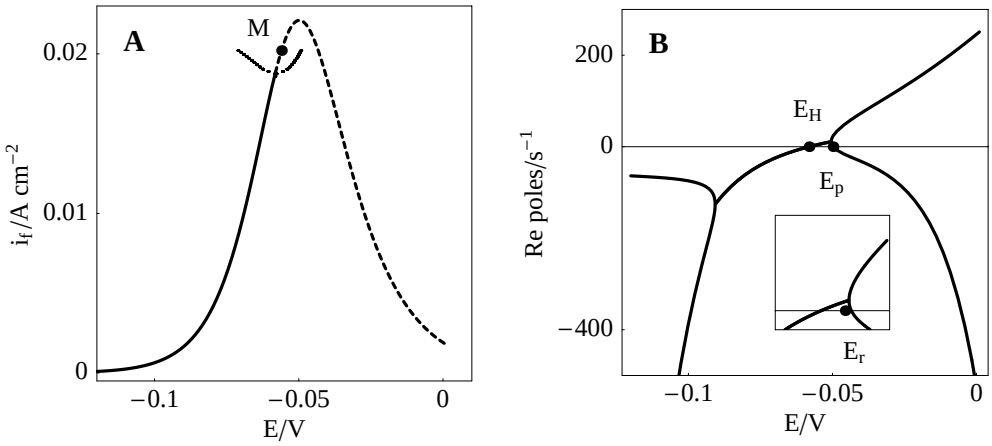

Figure 1:

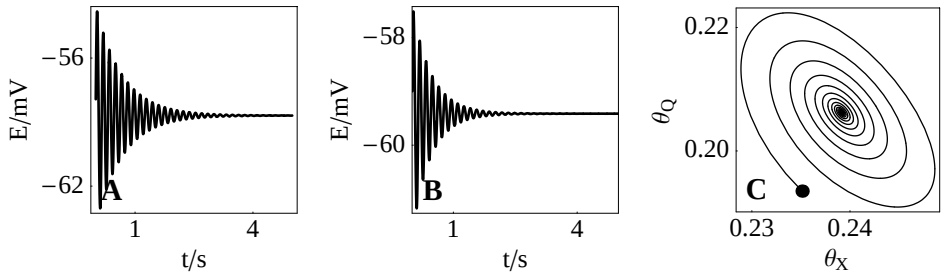

Figure 2:

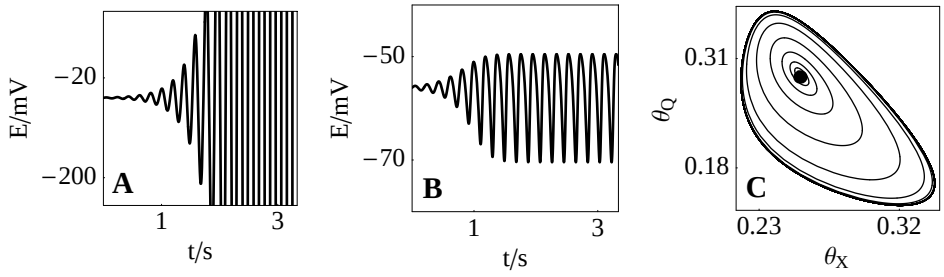

Figure 3:

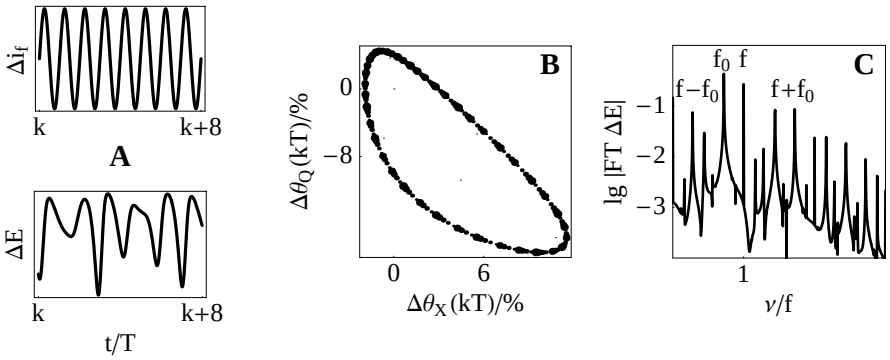

Figure 4:

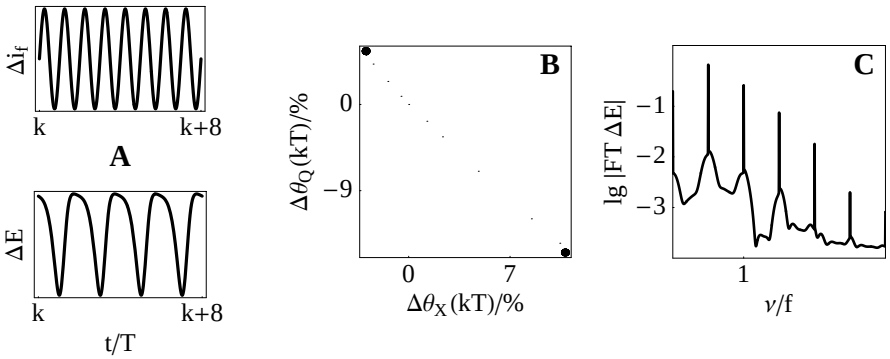

Figure 5:

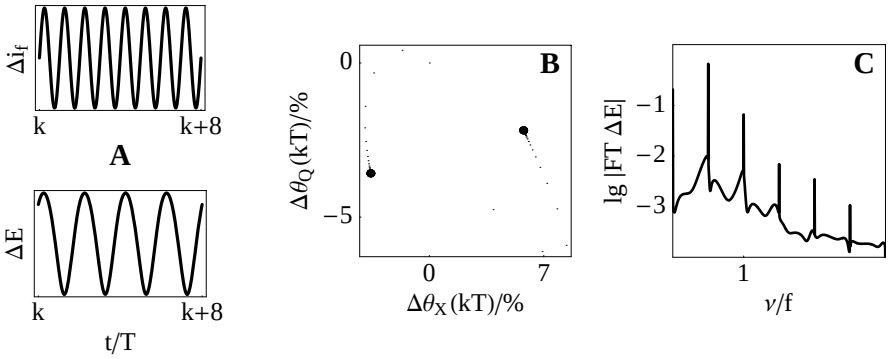

Figure 6:

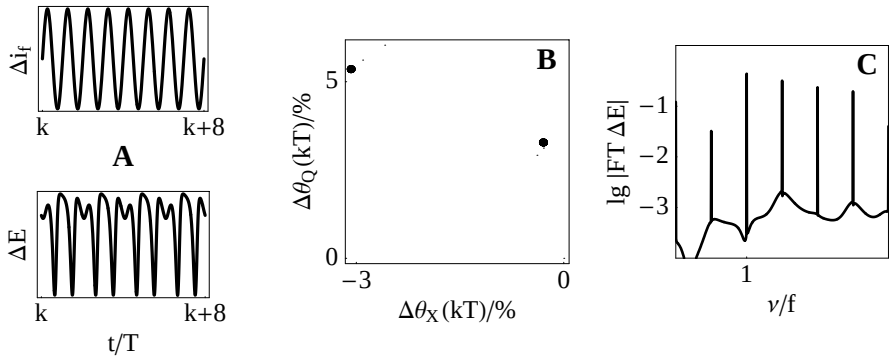

Figure 7:

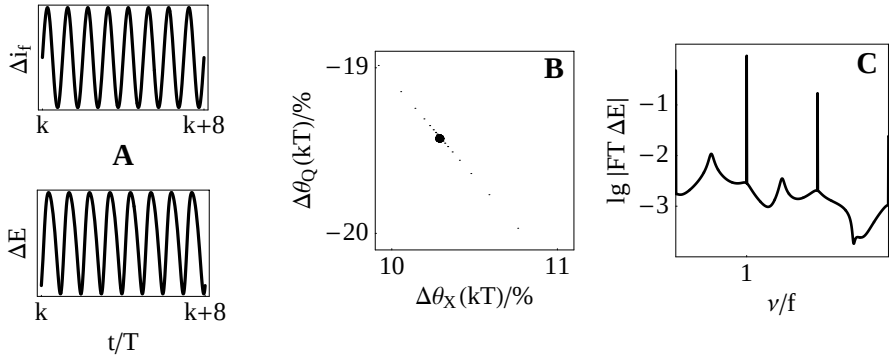

Figure 8:

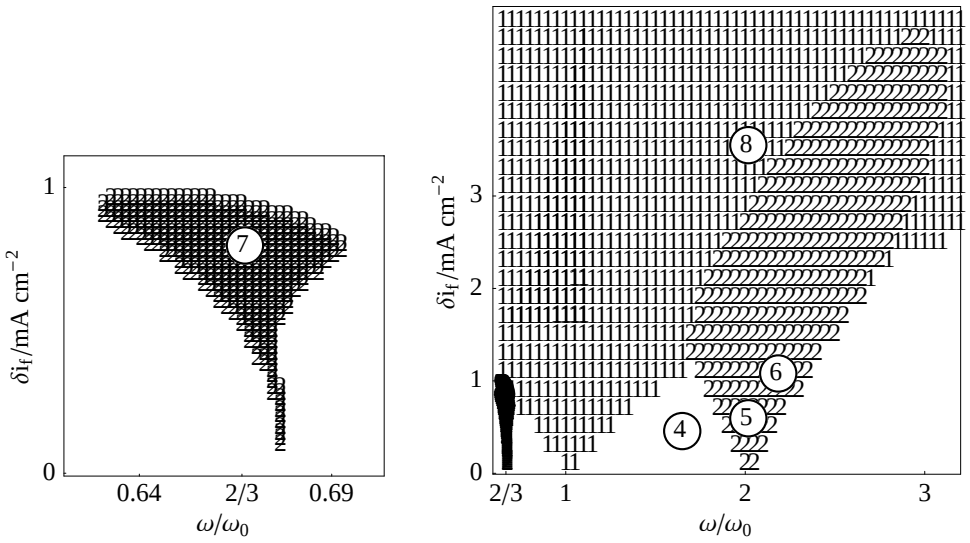

Figure 9: